A New NMR Crystallographic Approach to Reveal Calcium the Local Structure of Atorvastatin Calcium

Journal:	*Physical Chemistry Chemical Physics*
Manuscript ID	CP-ART-12-2018-007673.R1
Article Type:	Paper
Date Submitted by the Author:	21-Jan-2019
Complete List of Authors:	Holmes, Sean; University of Delaware, Chemistry and Biochemistry; University of Windsor, Chemistry and Biochemistry Wang, Wei David; Lanzhou University, State Key Laboratory of Applied Organic Chemistry, College of Chemistry and Chemical Engineering Hou, Guangjin; University of Delaware, Chemistry and Biochemistry Dybowski, Cecil; University of Delaware, Department of Chemistry and Bioche Wang, Wei; State Key Laboratory of Applied Organic Chemistry, Lanzhou University, College of Chemistry and Chemical Engineering Bai, Shi; University of Delaware, Chemistry and Biochemistry

A New NMR Crystallographic Approach to Reveal the Calcium Local Structure of Atorvastatin Calcium

Sean T. Holmes,[‡,†,a] Wei D. Wang,[‡,b] Guangjin Hou,[§,a] Cecil Dybowski,[a] Wei Wang,[*,b] and Shi Bai[*,a,b]

[a] Department of Chemistry and Biochemistry, University of Delaware, Newark, Delaware, 19716, USA
[b] State Key Laboratory of Applied Organic Chemistry, Lanzhou, Gansu, 730000, China
[‡] These authors contributed equally
[†] Current address: Department of Chemistry and Biochemistry, University of Windsor, Windsor, ON, N9B 3P4, Canada
[§] Current address: Dalian Institute of Chemical Physics, Chinese Academy of Sciences, Dalian, China
[*] Authors to whom correspondence should be addressed

Email: bais@udel.edu (S.B.) and wang_wei@lzu.edu.cn (W.W.)

Key Words: ^{43}Ca solid-state NMR; atorvastatin calcium trihydrate; quadrupolar NMR crystallography;

Abstract

We combine experimental and computational determinations of ^{43}Ca solid-state NMR parameters (chemical shift tensors, quadrupolar coupling tensors, and Euler angles) to constrain the structure of the local calcium–ligand coordination environment. A new ^{43}Ca NMR crystallographic approach which includes an extensive survey of the Cambridge Structural Database and a new symmetry benchmark is developed to enhance the selectivity of structural screening. The application of this method to quadrupolar NMR crystallographic investigations is demonstrated by unearthing calcium local structure of the active pharmaceutical ingredient atorvastatin calcium trihydrate, the active ingredient in Lipitor®, in the absence of diffraction data**.** This method has been tested by applying it to calcium acetate monohydrate which has a known structure.

Introduction

NMR crystallography is a nascent research field that combines solid-state NMR (SSNMR) spectroscopy and computational modelling with X-ray diffraction (XRD) to provide insight into molecular-level structure. Previous work in NMR crystallography[1-2] has focused on refining molecular structures derived from single-crystal[3-8] and/or powder XRD.[9] It is far more challenging to obtain crystal structures in the absence of diffraction data than to refine XRD-derived structures.[10-14] Chemical-shift (CS) and spin-diffusion data for spin-1/2 nuclei (*i.e.*, ^{1}H, ^{13}C, ^{15}N, and ^{19}F), have been used widely for structural refinement.[15-19] Quadrupolar ($I > 1/2$) nuclei,[20] like ^{14}N,[21] have been used less frequently as structural probes, although recent reports suggest that quadrupolar NMR parameters are useful for structural determination.[22-24]

When the crystalline solids contain ions such as sodium, chlorine, or calcium, analysis of the quadrupolar NMR powder patterns provides molecular-level structural information.[25-29] Quadrupolar line shapes are sensitive to local ion–ligand coordination chemistry; in particular, the electric-field-gradient (EFG) tensor components and its orientation with respect to the molecular frame are highly sensitive to local environments of the ions. Thus, analysis of quadrupolar line shapes may suggest key coordination chemistry and provide insights for conventional structural refinement of powder XRD data and/or aid in structural determinations in the absence of diffraction data.

As outlined in previous accounts,[30-34] the ^{43}Ca nucleus ($I = 7/2$, n.a. = 0.145%, and $\gamma = -1.8025 \times 10^{7}$ rad T^{-1} s^{-1}) is a sensitive structural probe. The ^{43}Ca central transition line shape depends strongly on the tensor character of both the chemical-shift and second-order quadrupolar interactions, the relative orientation of these interactions in the molecular

frame, and the strength of the applied magnetic field.[35-36] ^{43}Ca SSNMR spectroscopy has been applied to structural investigations of minerals,[35, 37-50] geopolymers,[51] glasses and slags,[52-57] cements,[58] metal organic frameworks,[59] and biologically-relevant solids.[60-64] ^{43}Ca SSNMR spectroscopy has played a crucial role in structural determination because of the sensitivity of calcium CS and EFG tensor parameters to structure.[42, 49, 62-63]

Among a variety of polymorphic and pseudopolymorphic forms,[65] Form I of atorvastatin calcium (ATC-I, **Fig. 1A**) is the active pharmaceutical ingredient of Lipitor®, which is commonly prescribed for lowering blood cholesterol and preventing hypertension or other cardiovascular diseases. The mechanism of atorvastatin inhibition of HMG-CoA reductase has been reported.[66] The crystal structure of ATC-I, which relates to bioavailability, stability, safety, and efficacy of the medication,[67] has not been determined. Our previous study[68] has revealed certain structural features of the atorvastatin ligands in ATC-I using multinuclear and multidimensional ^{13}C, ^{19}F, and ^{15}N SSNMR studies. A ^{43}Ca NMR study of ATC-I provides additional structural constraints, and could possibly aid in future structural determination.

Although solving a *complete* structure of ATC-I solely through SSNMR data is not practical at present, we develop herein a method of identifying the local symmetry at the calcium site and its coordination environment by combining ^{43}Ca SSNMR spectroscopy with computational chemistry. Our structural search begins with an extensive survey of calcium-containing crystals in the Cambridge Structural Database (CSD), followed by generation of a large library of candidates for the local calcium environment in ATC-I that meet certain energetic criteria. The library is strictly screened for matches with experimental ^{43}Ca NMR parameters using Hartree-Fock (HF) and density functional theory

(DFT) calculations. While the majority of models in the library are eliminated by comparison between calculated and experimental ^{43}Ca NMR chemical-shift and quadrupolar parameters, a number of structures cannot be differentiated with these comparisons alone. An analysis of the symmetry of the calcium site demonstrates that the line shape of the ^{43}Ca SSNMR powder pattern is very sensitive to β, the Euler angle between the most shielded CS principal axis (δ_{33}) and the major axis (V_{33}) of the EFG tensor. Thus, β is used as a new benchmark to eliminate remaining structural candidates in the library of candidate structures that do not meet the calcium site symmetry criterion.

To verify the applicability of this approach, we have applied it to calcium acetate monohydrate, which has a known single-crystal XRD structure. A correct structural motif in calcium acetate monohydrate has successfully been identified by this method.

Results and Discussion

Static and magic-angle-spinning (MAS) ^{43}Ca NMR spectra of ^{43}Ca-enriched ATC-I were collected at 19.97 T and 11.75 T (**Fig. 1B - 1E**). Because the second-order quadrupolar and anisotropic CS interactions both influence the ^{43}Ca line shape, spectral acquisition at two field strengths affords precise determination of NMR parameters.[31] The ^{43}Ca MAS pattern is narrow and nearly featureless at the higher field due to the diminution of the second-order quadrupolar broadening at high fields and averaging of the CS interaction under MAS conditions. Low-intensity bands are also observed in each MAS spectrum, corresponding to signals from the ±3/2 ⟷ ±5/2 satellite transitions.

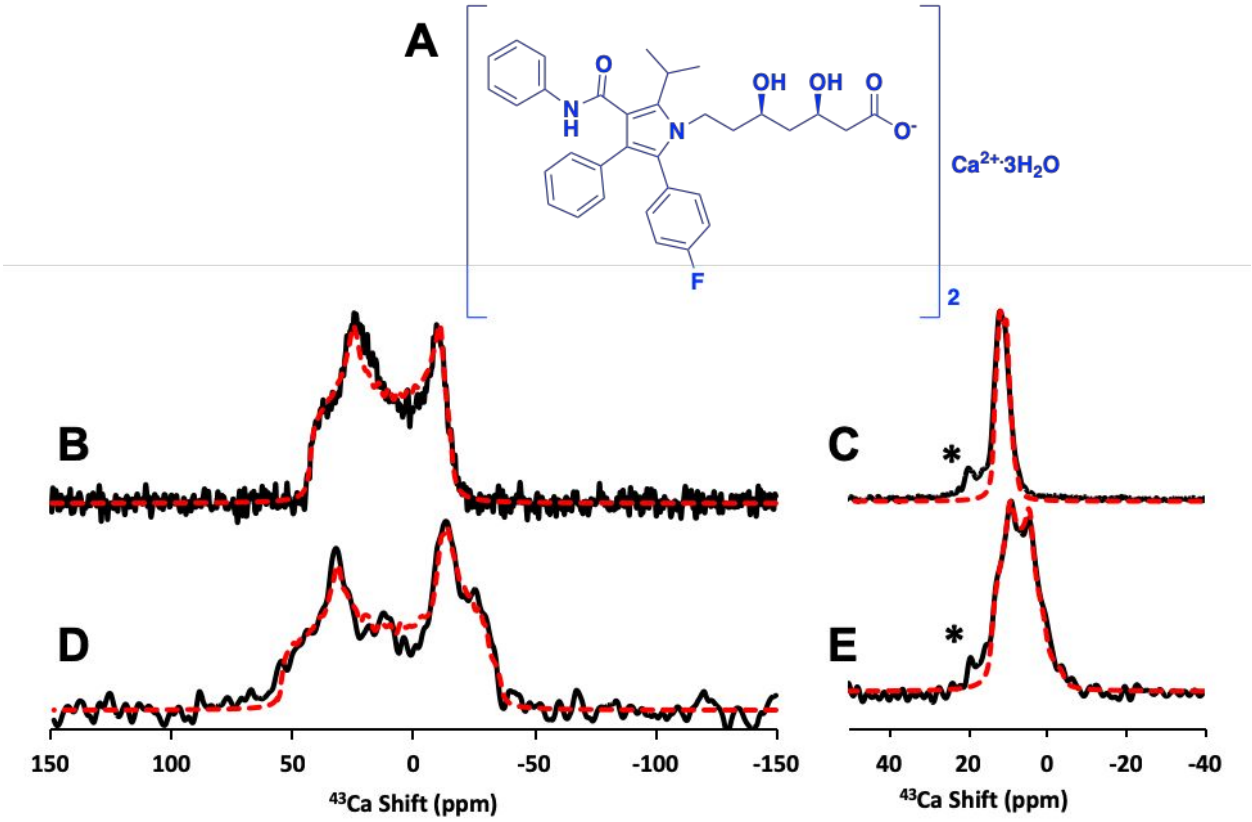

Fig. 1 Molecular structure of ATC-I (A) and ^{43}Ca NMR spectra (black) and spectral fittings (red dashes). Static (B, D) and MAS (C, E) spectra were acquired at 19.97 T (B, C) and 11.75 T (D, E), respectively. Asterisks in (C, E) indicate satellite transitions ±3/2 ↔ ±5/2.

Table 1. Experimental and Predicted ^{43}Ca NMR parameters for ATC-I [a-e]

	δ_{iso} (ppm)	$\Delta\delta$ (ppm)	η_{CSA}	C_Q (MHz)	η_Q	α (deg.)	β (deg.)	γ (deg.)
Exp.	15(1)	-27(2)	0.50(20)	1.81(15)	0.44(13)	58(3)	5(3)	27(3)
HF/cc-pVTZ	12.8	-32.7	0.62	2.10	0.21	121	9	299
PBE/cc-pVTZ	11.3	-34.1	0.48	1.93	0.19	124	13	304

[a] The experimental uncertainties in the last digit(s) for each value are indicated in parentheses. All calculations are based on model *m3_140* (See the text).
[b] Calculated magnetic shielding tensors were converted to the chemical shift scale *via* the referencing scheme outlined in the ESI.
[c] The isotropic chemical shift, chemical-shift anisotropy, and asymmetry parameter are given by $\delta_{iso} = (\delta_{11} + \delta_{22} + \delta_{33})/3$, $\Delta\delta = \delta_{33} - (\delta_{11} + \delta_{22})/2$, and $\eta_{CSA} = (\delta_{22} - \delta_{11})/(\delta_{33} - \delta_{iso})$, respectively. The principal values of the CS tensor are ranked $\delta_{11} \geq \delta_{22} \geq \delta_{33}$.
[d] The quadrupolar coupling constant and asymmetry parameter are given by $C_Q = eQV_{33}/h$ and $\eta_Q = (V_{11} - V_{22})/V_{33}$, respectively. The sign of C_Q cannot be determined from the experimental ^{43}Ca spectra. The principal values of the EFG tensors are ranked $|V_{33}| \geq |V_{22}| \geq |V_{11}|$.
[e] The Euler angles α, β, and γ define the relative orientation of the CS and EFG tensors, using the convention described in the ESI.

Simulations of the ^{43}Ca patterns show that ATC-I contains a single calcium site with a chemical-shift parameter set of $\delta_{iso} = 15 \pm 1$ ppm, $\Delta\delta = -27 \pm 2$ ppm, and $\eta_{CSA} = 0.50 \pm 0.20$ and ~~an~~ EFG tensor components of $C_Q = 1.81 \pm 0.15$ MHz and $\eta_Q = 0.44 \pm 0.13$ (**Table 1**). The Euler angles between the orientations of the principal-axis systems of the EFG tensor and the CS tensor are $\alpha = 58 \pm 3°$, $\beta = 5 \pm 3°$, and $\gamma = 27 \pm 3°$. We note that multiple sets of α and γ produce similar ^{43}Ca line shapes, within reasonable accuracy, as long as β is close to 0° and $\alpha + \gamma$ is close to 90°, 180°, or 270°; a representative value of $\alpha + \gamma = 85°$ with the smallest error is given here (*vide infra*).

The calcium coordination number and the average Ca–O distance are correlated with δ_{iso}(^{43}Ca) such that a value of 15 ppm suggests an average Ca–O distance of *ca.* 2.4 Å and a coordination number between 6 and 9.[32, 37] The values of C_Q (1.81 MHz) and $\Delta\delta$ (-27 ppm) are typical values for calcium carboxylates.[38] Unlike other calcium carboxylate

hydrates,[39, 63] the small value of β (5°) implies that the directions of the *33* axes of the ^{43}Ca CS and EFG tensors are nearly coaxial in ATC-I.

We assume that the local calcium structure in ATC-I adopts a coordination chemistry similar to one of the *ca.* 2800 calcium environments found in the CSD. Of these environments, 103 consist of at least one carboxylate ligand and one water molecule. They can be grouped into 14 distinct bonding *motifs* based on the number and types of ligands bound to the calcium ion (**Table S1**). Appropriate candidate structures for ATC-I must be consistent with the overall stoichiometry of Ca(atorvastatin)$_2\cdot 3H_2O$, have a plausible combination of terminal and bridging ligands, and possess a coordination number in agreement with $\delta_{iso}(^{43}Ca)$. Only *three* structural motifs (*m1*: $Ca(COO)_4\cdot 2H_2O$, *m2*: $Ca(COO)_3\cdot 3H_2O$, and *m3*: $Ca(COO)_3\cdot 4H_2O$) are considered to be suitable candidates for ATC-I (**Fig. 2A - 2C**). These three motifs are ranked as the first, second, and fifth, in terms of the number of occurrences in the CSD survey (see ESI for details).

Initial structural candidates for ATC-I were constructed using three geometry-optimized motifs where acetate serves as a surrogate for the bulky atorvastatin ligand (**Fig. 2A – 2C**). Calculations on these initial structures produce large deviations from experimental NMR parameters, indicating that further structural refinement is required (**Table S2**). Calculation on a model based on the known crystal structure of calcium dibenzoate trihydrate,[63] which was used as a "convenient model" for ATC-I,[68] also failed to predict the experimental ^{43}Ca NMR parameters.

Bond lengths (Ca–O), bond angles (O–Ca–O and Ca–O–C), and dihedral angles (O–Ca–O–C and O–Ca–O–H) of the three initial structural motifs were varied using a random-walk procedure to create a library of candidate structures. Acetate ligands and water

molecules were treated as rigid bodies. The relative positions of ligands were sampled with a maximum step size of 0.2 Å for bond lengths and 25° for bond angles and dihedral angles. The nuclear-repulsion energy calculated for each randomly generated structure was used as a benchmark for retaining a candidate structure. This first stage of screening eliminated structures with overlapping ligands or structures in which the ligands were too close to the calcium ion. The random-walk procedure and energy screening were continued until 333 acceptable configurations were produced for each motif, resulting in a library of 999 possible structures for ATC-I. We use *m1*, *m2*, and *m3* to denote the three structural motifs and an index between 1 and 333 to denote the entry number within that motif.

^{43}Ca CS and EFG tensors for the 999 structural candidates were calculated at the HF/cc-pVDZ level, resulting in a broad distribution of the NMR parameters (-80 ppm < δ_{iso} < 70 ppm; -150 ppm < $\Delta\delta$ < -5 ppm; and 0.1 MHz < $|C_Q|$ < 8.1 MHz). The distributions in the NMR parameters and the reduced-χ statistics (*vide infra*) indicate that the library of candidate structures possesses a random distribution of structural features and is statistically significant (**Fig. 2A – 2D**).[23]

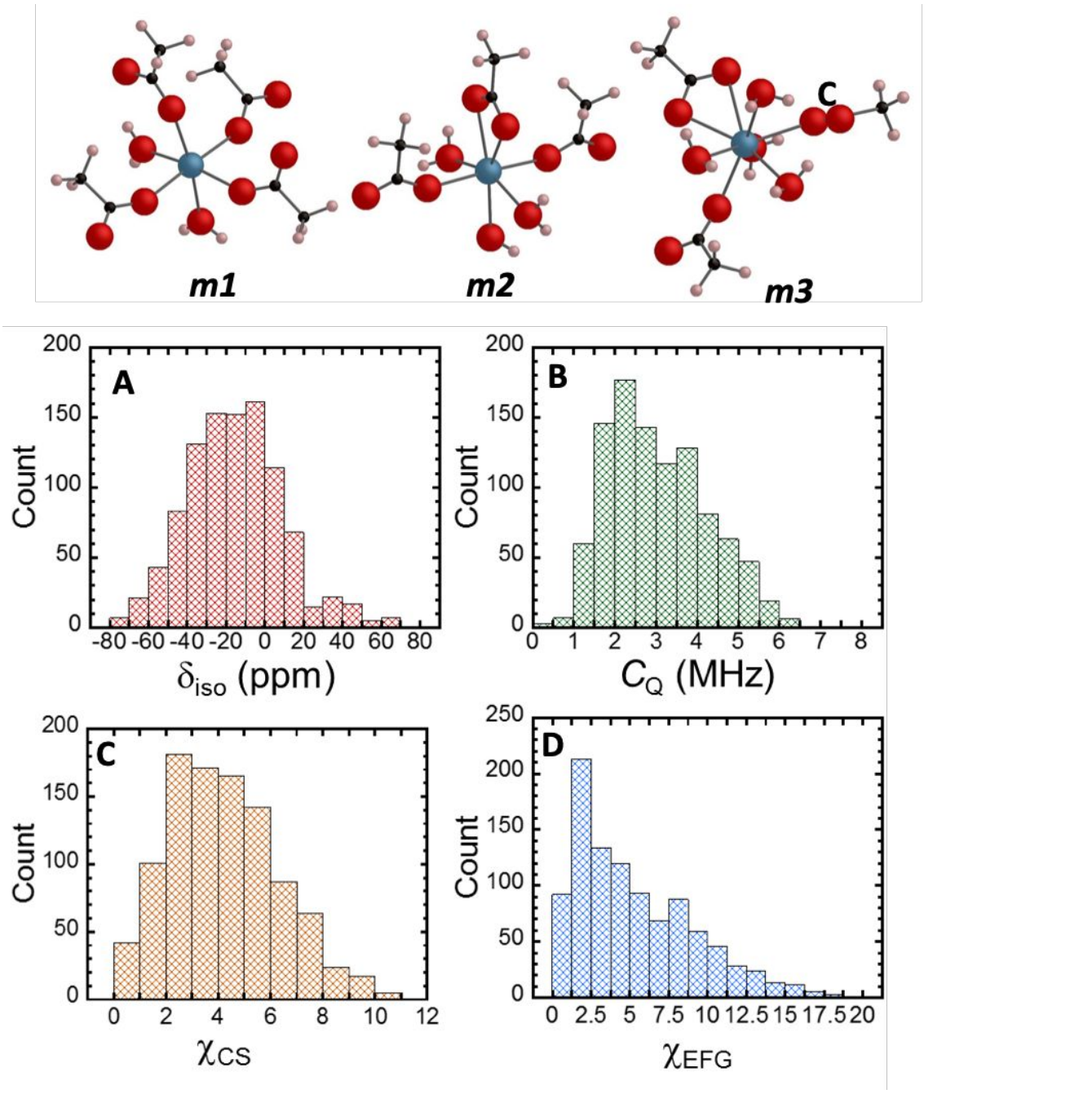

Fig. 2 Energy-minimized structures representing the three structure motifs (*m1-m3*) for ATC-I as obtained at the HF/cc-pVDZ level. Distributions of calculated ^{43}Ca (A) δ_{iso}, (B) C_Q, (C) χ_{CS}, and (D) χ_{EFG} for the library of candidate structures of ATC-I. All ^{43}Ca NMR parameters were calculated at the HF/cc-pVDZ level.

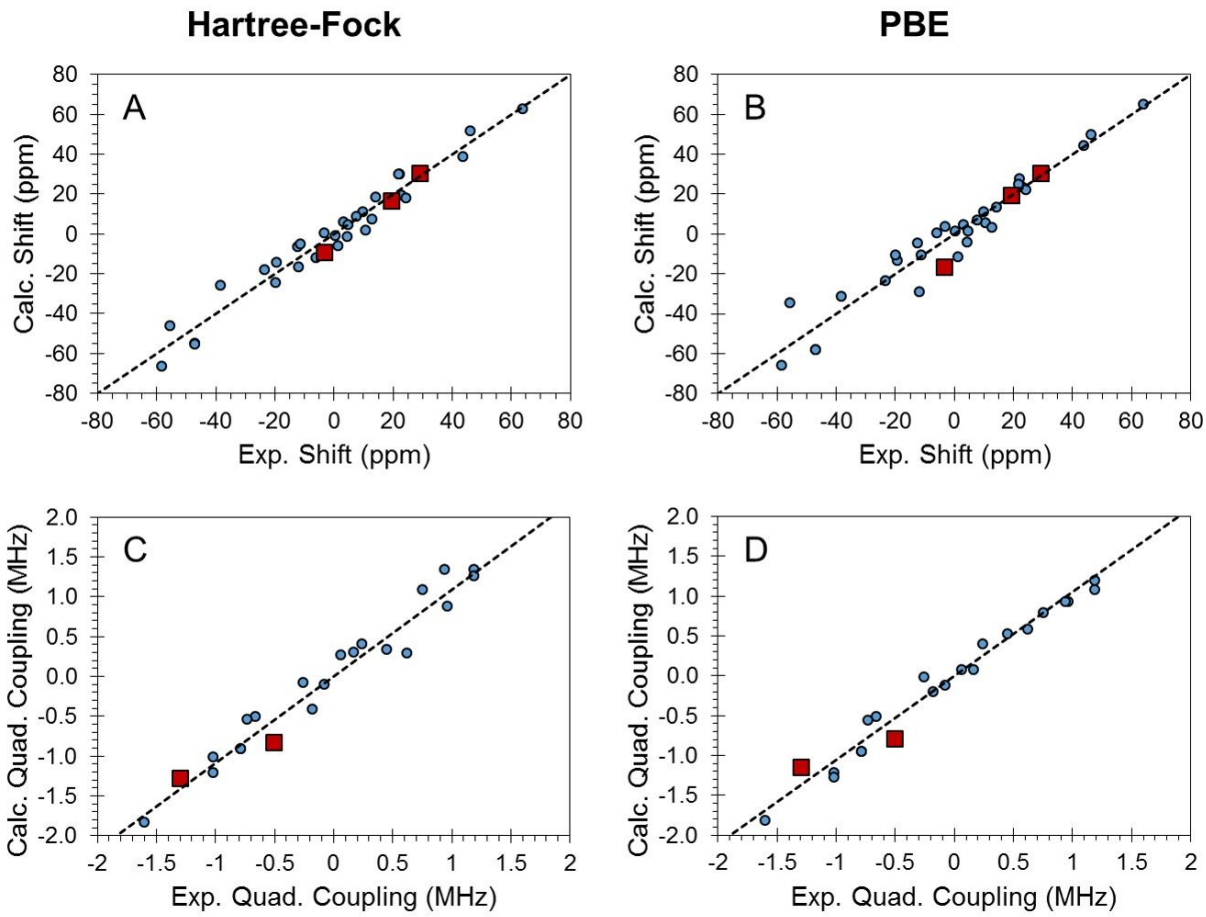

Fig. 3. Correlation between the three principal components of calculated and experimental calcium chemical shift tensors (A, B), and between two principal components (eQV_{11}/h and eQV_{22}/h) of calculated and experimental calcium quadrupolar coupling tensors (C, D). These calculations were performed at the HF/cc-pVTZ and PBE/cc-pVTZ levels. Blue markers indicate the values obtained from calculations based on 10 calcium-containing compounds with known structures from the literature, whereas red markers indicate calculations on *m3_140*. These compounds are calcium formate, calcium acetate monohydrate (two sites), calcium tartrate tetrahydrate, calcium dibenzoate trihydrate, calcite, aragonite, $Ca(NO_3)_2$, $CaSO_4 \cdot 2H_2O$, and $CaCl_2 \cdot 2H_2O$.

In our recent work, we have analyzed the accuracy of calculated ^{43}Ca SSNMR parameters for ten solids with known crystal structures; the errors established therein allow one to screen the library of candidate structures for matches with experiment (**Fig. 3**).[23] Application of reduced-χ statistics allowed elimination of 930 structures at the 99% confidence level, using either CS or EFG tensor parameters (**Table 2**). As expected, the

remaining 69 model structures showed a narrowed distribution of ^{43}Ca NMR parameters (-32 ppm < δ_{iso} < 7 ppm; -44 ppm < $\Delta\delta$ < -12 ppm; and 0.9 MHz < $|C_Q|$ < 2.7 MHz). A combination of geometry optimization of the remaining structures and calculation of the NMR parameters at the HF/cc-pVTZ level resulted in elimination of 47 additional structures at 95% confidence. DFT calculations (PBE/cc-pVTZ), reportedly improved for ^{43}Ca EFG tensor prediction,[23] led to further elimination of 6 structures at 95% confidence. Following these stages of structural screening, a total of 16 structures remained that were indistinguishable by reduced-χ statistics (**Table S3**). We note that application of other statistical metrics such as *t*-test results in comparably selective screening of candidate structures.

Table 2. Structural screening for ATC-I

	No. of Surviving Structures			
Screening Method	*m1*	*m2*	*m3*	Total
Nuclear repulsion energy	333	333	333	**999**
NMR parameters, HF/cc-pVDZ; χ < 2.57	26	7	36	**69**
Geometry optimization, HF/cc-pVDZ [a]	25	7	35	**67**
NMR parameters, HF/cc-pVTZ; χ < 1.96	7	0	15	**22**
NMR parameters, PBE/cc-pVTZ; χ < 1.96	6	0	10	**16**
Euler angle β	0	0	1	**1**

[a] Geometry optimizations failed to converge for two candidates. All subsequent NMR calculations were performed on the energy-minimized structures.

Simulated ^{43}Ca NMR powder patterns,[69] using calculated CS tensors, EFG tensors, and Euler angles, for the sixteen surviving candidate structures varied significantly from model to model (**Fig. 4**). Only one structure (*m3_140,* **Fig. 5A**), with the smallest value of β (9° by HF/cc-pVTZ and 13° by PBE/cc-pVTZ), features a ^{43}Ca NMR line shape consistent with the experimental pattern. This result indicates that comparison of experimental and

calculated Euler angles serves as a powerful benchmark with which to assess proposed structural models of ATC-I.

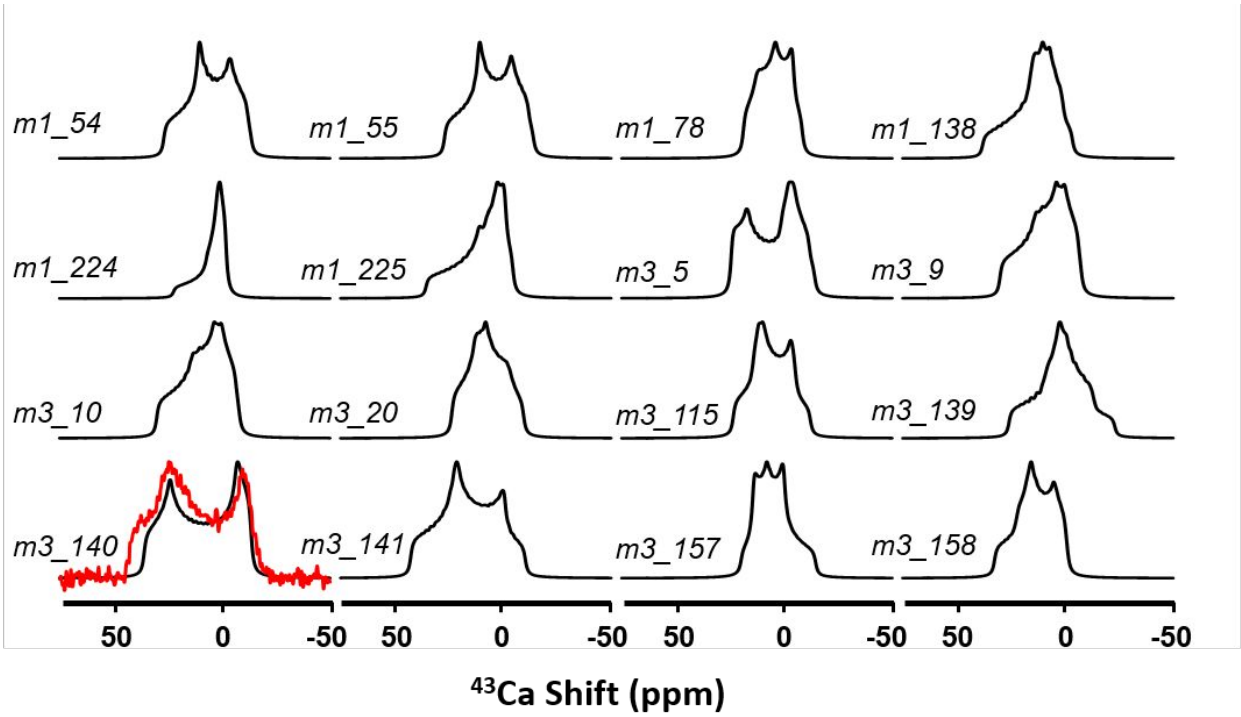

Fig. 4 Simulated ^{43}Ca patterns (19.97 T) of the sixteen retained structures after reduced-χ screening. The experimental data (red) are overlaid with *m3_140*.

Further simulations suggest that the ^{43}Ca line shapes are sensitive to β when $\alpha + \gamma$ is kept constant at 85° (near 90°) (**Fig. 5B**), which allows one to use β as a critical new symmetry benchmark in the structural search. To understand the critical role of β in the structural screening, the symmetry at the calcium site, reflected by the ^{43}Ca NMR line shapes, has been analyzed. For two special cases, where $\beta = 0°$ and $\alpha + \gamma = 180°$ or 90°/270°, the simulated NMR patterns are indistinguishable (**Fig. S3**). These two cases correspond to a calcium ion with local C_{2v} point-group symmetry. The observed Euler angles ($\beta = 5°$ and $\alpha + \gamma = 85°$) imply that the local symmetry of the calcium site in ATC-I approaches C_{2V},

which is consistent with the proposed model *m3_140*. A more detailed account of this analysis is provided in the ESI.

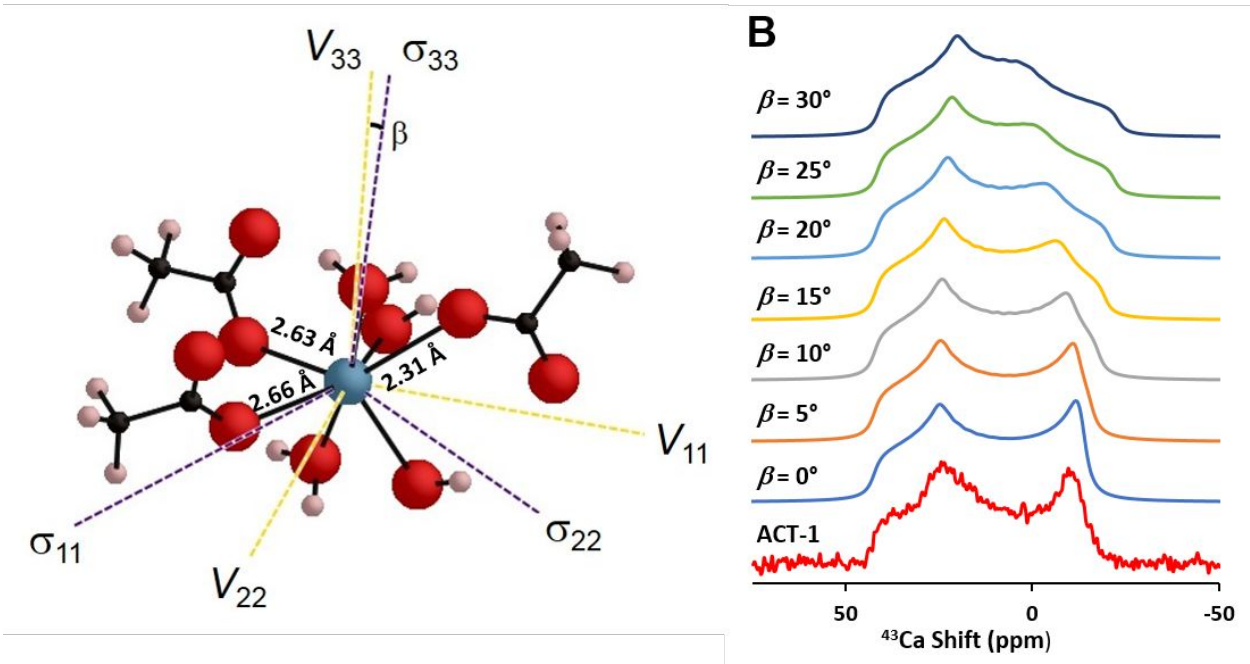

Fig. 5 (A) The proposed structure, *m3_140,* of ATC-I. (B) Variation of β has a significant impact of the ^{43}Ca line shapes at 19.97 T. Experimental CS and EFG tensor parameters and Euler angles (α = 58° and γ = 27°) were used in the simulations. The experimental ^{43}Ca pattern at 19.97 T (red) is shown for comparison.

m3_140 has a coordination number of 8 and an average Ca–O bond length of 2.41 Å, consistent with those predicted by the experimental value of $\delta_{iso}(^{43}Ca)$. In *m3_140*, the calcium ion coordinates with four waters and three acetate ligands. Of the acetate ligands, two feature similar Ca–O bond lengths (2.63 Å and 2.66 Å). The third Ca–O bond length is 2.31 Å (**Table S6**), implying it is a terminal ligand, whereas the others are bridging. In addition, two water molecules are expected to serve as bridging ligands between calcium sites.

^{13}C SSNMR spectroscopy has identified two types of carboxylic carbons in ATC-I having values of $\delta_{iso}(^{13}C)$ separated by 4.2 ppm.[68] Calculation on an augmented *m3_140*

structure (**Fig. S8**) at the HF/cc- pVTZ level yields two distinguishable carboxylic carbon chemical shifts differing by 5.2 ppm, further validating the proposed structure. Calculation on the augmented model also results in reasonably accurate predictions of the principal values of the ^{13}C chemical shift tensors (**Table S7**).

Independently, this protocol has also been applied "blindly" to predict the local structure of the Ca2 site of calcium acetate monohydrate which has been determined independently by single-crystal XRD.[38] Following the same procedures as was used to predict a suitable model for ATC-I, five similar candidate structures were identified and they all belong to *m1* (**Table S8**). The XRD structure[70] confirms that Ca2 in calcium acetate monohydrate also belongs to *m1*. The structures of calcium acetate monohydrate were obtained by limiting our selection to models in which β was near 90°, as opposed to our analysis of ATC-I which selected models with β near 0°. Comparison between the structures derived from single-crystal XRD and through the NMR-based screening protocol is provided in **Fig. S9**. The protocol is thus validated through the structure search for calcium acetate monohydrate.

Conclusion

Without preliminary knowledge of either the extended crystal structure of ATC-I or the local coordination environment of the calcium ion, we have proposed a calcium local structure that is consistent with structural constraints imposed by ^{43}Ca SSNMR spectra. Because the origins of the CS and QC interactions are different, calculated parameters serve as orthogonal figures of merit for assessing candidate structures. Furthermore, since the Euler angles between the principal coordinate systems of the CS and EFG tensors are ~~a~~

highly sensitive symmetry benchmarks, they can be used readily to single out the most plausible structure from a large library of candidate structures. Based on this analysis, a local point group symmetry approaching C_{2v} for the calcium site in ATC-I has been determined and the key geometric constraints in our model structure have been verified to be consistent with those of ATC-I. It is possible that the structural constraints determined in this study could be used in combination with high-resolution PXRD data to determine the complete crystal structure of ATC-I. This protocol has been applied independently to propose a local structure for one of the calcium ions in calcium acetate monohydrate, where the structure is known from single-crystal XRD.

These examples indicate that accurate determination of the full CS and EFG tensor components *as well as* their relative orientations enabled a *new* highly-selective and robust structural search tool for a local crystallographic structure. This is accomplished by introducing a structural model that satisfies constraints indicated by the values of the NMR parameters and symmetry criteria embedded in the experimental NMR line shape. This general structure-searching method, in principle, can be readily applied to NMR crystallographic investigations of materials containing quadrupolar ions in which the quadrupolar and ~~the~~ anisotropic CS interactions are comparable in size, and particularly where the relative orientation, expressed in terms of Euler angles, between these interactions has a significant impact on the quadrupolar line shapes.

Experimental and Computational Methods

Sample Preparation. 50 mg of $CaCO_3$ (Cambridge Isotope Laboratories), enriched at 62.2% in ^{43}Ca, was calcined at 1173 K for 5 h to form ^{43}CaO. The ^{43}CaO was suspended in 1 mL of water.

25 mL of an aqueous solution of atorvastatin acid (Quzhou Aifeimu Chemical Co., Ltd.) was added dropwise to the suspension. After stirring for 1.5 h at 343 K, the resulting solution was cooled to room temperature, filtered, and washed three times with diethyl ether, with a yield of approximately 60%. Characterization of labelled and natural abundance samples of ATC-I was accomplished through PXRD and ^{13}C CP/MAS SSNMR spectroscopy (**Figs. S1 – S2**). The PXRD patterns demonstrate that the sample studied in the present work is ATC-I *via* comparison with the PXRD patterns previously reported.[71]

Powder X-ray Diffraction. PXRD patterns of ATC-I were recorded using a PANalytical X'Pert PRO diffractometer with a Cu K_α radiation source (1.54056 Å). Data were collected in continuous mode with a step size of 0.02° and step time of 10 s, over a 2θ range of 3 - 50° at 298 K. The X-ray tube voltage and amperage were 40 kV and 40 mA.

Solid-state NMR Spectroscopy. ^{43}Ca NMR spectra were obtained at 19.97 T and 11.75 T with Bruker Avance III solid-state NMR spectrometers, operating with $\nu_0(^{43}Ca)$ = 57.23 MHz and $\nu_0(^{43}Ca)$ = 33.66 MHz, respectively. Bruker 3.2 mm (19.97 T) or 4.0 mm HX (11.75 T) low-γ MAS probes were used for static and MAS measurements at 298 K. For MAS experiments, the spinning frequencies were regulated at 18.000 ± 0.003 kHz (19.97 T) or 10.000 ± 0.003 kHz (11.75 T), using ~~the~~ Bruker MAS controller. All experiments used a relaxation delay of 4 s. The numbers of scans were 20,000 and 10,000 for static and MAS experiments, respectively. A 1.00 M $CaCl_2$ solution was used as the external CS reference for all ^{43}Ca spectra. ^{13}C CP/MAS spectra of ATC-I were acquired with a Bruker AVANCE II WB400 NMR spectrometer, operating with $\nu_0(^1H)$ = 400.13 MHz and $\nu_0(^{13}C)$ = 125.50 MHz. Samples were packed in 4 mm rotors, a HX probe was used, and all spectra were obtained at 298 ± 2 K. The ^{13}C CP/MAS experiments were carried out with a sample spinning rate of 10.000 ± 0.003 kHz. Two-pulse phase-modulated decoupling during

CP/MAS data acquisition was provided by a 104.2 kHz ^{1}H decoupling field with a contact time of 3 ms. All ^{13}C chemical shifts were referenced externally to tetramethylsilane *via* the resonance of adamantane at an isotropic chemical shift of 38.55 ppm.

Spectral Simulations. The static and MAS ^{43}Ca NMR spectra were fit using a FORTRAN code developed in our laboratory. The ^{43}Ca CS tensor, QC tensor, and Euler angles of ATC-I were obtained by fitting two spectra acquired at different fields simultaneously for improved spectral simulation accuracy. Additional numerical simulations of the effect of the choice of Euler angles on the NMR line shape were performed using SIMPSON.[69]

Survey of Cambridge Structural Database. The survey of calcium-containing solids deposited within the CSD utilized the software packages ConQuest (version 1.19) and Mercury (version 3.9).

Computational Details. All calculations employed GAUSSIAN 09.[72] Geometry optimizations were performed at the HF level using the cc-pVDZ basis set,[73] and led to energy-minimized structures by relaxing the positions of all atoms in the models that are not directly bound to the calcium ions. Calculations of NMR parameters were performed at the HF or PBE levels,[74] using the cc-pVDZ or cc-pVTZ basis sets. Electrostatic embedding was used in all calculations to model the contributions of long-range polarization, as described through the integral-equation formalism of the polarizable-continuum model (IEFPCM),[75-76] in which atomic radii and non-Coulomb terms were computed by the SMD algorithm using water as the solvent.[77] Magnetic-shielding tensors were calculated within the GIAO formalism, as implemented in GAUSSIAN 09. Calculated magnetic-shielding parameters were converted to the CS scale using the referencing scheme discussed in the ESI. Euler angles were extracted from the GAUSSIAN 09 output files using EFGShield.[78]

Conflicts of Interest

There are no conflicts to declare.

Acknowledgements

This publication was made possible by the Delaware COBRE program NIGMS (5 P30 GM110758-02) from the National Institute of Health. W.W. acknowledges the support of the 111 Project (111-2-17). C.D. acknowledges the support if the National Sciences Foundation under DMR-1608366. S.B. and S.T.H acknowledge the late Dr. Alexander J. Vega for helpful discussion.

References

1. S. E. Ashbrook and D. McKay, *Chem. Commun.*, 2016, **52**, 7186-7204.
2. G. J. Beran, J. D. Hartman and Y. N. Heit, *Acc. Chem. Res.*, 2016, **49**, 2501-2508.
3. K. Kalakewich, R. Iuliucci, K. T. Mueller, H. Eloranta and J. K. Harper, *J. Chem. Phys.*, 2015, **143**, 194702.
4. M. Baias, J. N. Dumez, P. H. Svensson, S. Schantz, G. M. Day and L. Emsley, *J. Am. Chem. Soc.*, 2013, **135**, 17501-17507.
5. J. K. Harper, R. Iuliucci, M. Gruber and K. Kalakewich, *CrystEngComm*, 2013, **15**, 8693-8704.
6. D. H. Brouwer, *J. Magn. Reson.*, 2008, **194**, 136-146.
7. D. H. Brouwer, I. L. Moudrakovski, R. J. Darton and R. E. Morris, *Magn. Reson. Chem.*, 2010, **48**, S113-S121.
8. D. H. Brouwer and G. D. Enright, *J. Am. Chem. Soc.*, 2008, **130**, 3095-3105.
9. C. Martineau, A. Cadiau, B. Bouchevreau, J. Senker, F. Taulelle and K. Adil, *Dalton Trans.*, 2012, **41**, 6232-6241.
10. C. Yang, L. Zhu, R. A. Kudla, J. D. Hartman, R. O. Al-Kaysi, S. Monaco, B. Schatschneider, A. Magalhaes, G. J. O. Beran, C. J. Bardeen and L. J. Mueller, *CrystEngComm*, 2016, **18**, 7319-7329.
11. K. Kalakewich, R. Iuliucci and J. K. Harper, *Cryst. Growth Des.*, 2013, **13**, 5391-5396.
12. G. M. Day, *Crystallogr Rev*, 2011, **17**, 3-52.
13. C. J. Pickard and R. J. Needs, *J Phys-Condens Mat*, 2011, **23**.
14. J. K. Harper and D. M. Grant, *Cryst. Growth Des.*, 2006, **6**, 2315-2321.
15. R. K. Harris, P. Y. Ghi, H. Puschmann, D. C. Apperley, U. J. Griesser, R. B. Hammond, C. Ma, K. J. Roberts, G. J. Pearce, J. R. Yates and C. J. Pickard, *Org. Process Res. Dev.*, 2005, **9**, 902-910.
16. R. K. Harris, *J. Pharm. Pharmacol.*, 2007, **59**, 225-239.

17. Y. Garro Linck, A. K. Chattah, R. Graf, C. B. Romanuk, M. E. Olivera, R. H. Manzo, G. A. Monti and H. W. Spiess, *Physical Chemistry Chemical Physics*, 2011, **13**, 6590-6596.
18. A. Abraham, D. C. Apperley, T. Gelbrich, R. K. Harris and U. J. Griesser, *Can. J. Chem.*, 2011, **89**, 770-778.
19. W. Liu, W. D. Wang, W. Wang, S. Bai and C. Dybowski, *J. Phys. Chem. B*, 2010, **114**, 16641-16649.
20. P. Pyykkö, *Molecular Physics*, 2008, **106**, 1965-1974.
21. S. L. Veinberg, K. E. Johnston, M. J. Jaroszewicz, B. M. Kispal, C. R. Mireault, T. Kobayashi, M. Pruski and R. W. Schurko, *Phys. Chem. Chem. Phys.*, 2016, **18**, 17713-17730.
22. S. T. Holmes and R. W. Schurko, *J. Phys. Chem. C*, 2018, **122**, 1809-1820.
23. S. T. Holmes, S. Bai, R. J. Iuliucci, K. T. Mueller and C. Dybowski, *J. Comput. Chem.*, 2017, **38**, 949-956.
24. F. A. Perras and D. L. Bryce, *The Journal of Physical Chemistry C*, 2012, **116**, 19472-19482.
25. A. A. Peach, D. A. Hirsh, S. T. Holmes and R. W. Schurko, *CrystEngComm*, 2018.
26. K. M. N. Burgess, F. A. Perras, A. Lebrun, E. Messner-Henning, I. Korobkov and D. L. Bryce, *J. Pharm. Sci.*, 2012, **101**, 2930-2940.
27. H. Hamaed, J. M. Pawlowski, B. F. T. Cooper, R. Fu, S. H. Eichhorn and R. W. Schurko, *J. Am. Chem. Soc.*, 2008, **130**, 11056-11065.
28. A. M. Namespetra, D. A. Hirsh, M. P. Hildebrand, A. R. Sandre, H. Hamaed, J. M. Rawson and R. W. Schurko, *CrystEngComm*, 2016, **18**, 6213-6232.
29. F. A. Perras and D. L. Bryce, *Angew Chem Int Edit*, 2012, **51**, 4227-4230.
30. R. W. Schurko and M. J. Jaroszewicz, in *Encyclopedia of Inorganic and Bioinorganic Chemistry*, John Wiley & Sons, Ltd2011.
31. D. Laurencin and M. E. Smith, *Prog. Nucl. Magn. Reson. Spectrosc.*, 2013, **68**, 1-40.
32. D. L. Bryce, *J. Chem. Soc., Dalton Trans.*, 2010, **39**, 8593-8602.
33. A. Wong, P. M. Aguiar, T. Charpentier and D. Sakellariou, *Chem. Sci.*, 2011, **2**, 815-818.
34. C. M. Widdifield, 2017, pp. 227-363.
35. D. L. Bryce, E. B. Bultz and D. Aebi, *J Am Chem Soc*, 2008, **130**, 9282-9292.
36. D. Laurencin, C. Gervais, A. Wong, C. Coelho, F. Mauri, D. Massiot, M. E. Smith and C. Bonhomme, *J Am Chem Soc*, 2009, **131**, 13430-13440.
37. R. Dupree, A. P. Howes and S. C. Kohn, *Chem. Phys. Lett.*, 1997, **276**, 399-404.
38. C. M. Widdifield, I. Moudrakovski and D. L. Bryce, *Phys. Chem. Chem. Phys.*, 2014, **16**, 13340-13359.
39. K. M. N. Burgess, Y. Xu, M. C. Leclerc and D. L. Bryce, *Inorg. Chem.*, 2014, **53**, 552-561.
40. K. M. N. Burgess, F. A. Perras, I. L. Moudrakovski, Y. Xu and D. L. Bryce, *Can. J. Chem.*, 2015, 1-9.
41. K. M. N. Burgess and D. L. Bryce, *Solid State Nucl. Magn. Reson.*, 2015, **65**, 75-83.
42. D. Laurencin, A. Wong, J. V. Hanna, R. Dupree and M. E. Smith, *J. Am. Chem. Soc.*, 2008, **130**, 2412-2413.
43. P. Gras, A. Baker, C. Combes, C. Rey, S. Sarda, A. J. Wright, M. E. Smith, J. V. Hanna, C. Gervais, D. Laurencin and C. Bonhomme, *Acta Biomater.*, 2016, **31**, 348-357.
44. C. M. Widdifield and D. L. Bryce, *Can. J. Chem.*, 2011, **89**, 754-763.
45. Y.-C. Huang, Y. Mou, T. W.-T. Tsai, Y.-J. Wu, H.-K. Lee, S.-J. Huang and J. C. C. Chan, *J. Phys. Chem. B*, 2012, **116**, 14295-14301.
46. J. W. Singer, A. Ö. Yazaydin, R. J. Kirkpatrick and G. M. Bowers, *Chem. Mater.*, 2012, **24**, 1828-1836.
47. D. Laurencin, A. Wong, R. Dupree and M. E. Smith, *Magn. Reson. Chem.*, 2008, **46**, 347-350.
48. A. Wong, D. Laurencin, R. Dupree and M. E. Smith, *Solid State Nucl. Magn. Reson.*, 2009, **35**, 32-36.

49. M. Reinholdt, J. Croissant, L. Di Carlo, D. Granier, P. Gaveau, S. Bégu, J.-M. Devoisselle, P. H. Mutin, M. E. Smith, C. Bonhomme, C. Gervais, A. van der Lee and D. Laurencin, *Inorg. Chem.*, 2011, **50**, 7802-7810.
50. C. Gervais, D. Laurencin, A. Wong, F. Pourpoint, J. Labram, B. Woodward, A. P. Howes, K. J. Pike, R. Dupree, F. Mauri, C. Bonhomme and M. E. Smith, *Chem. Phys. Lett.*, 2008, **464**, 42-48.
51. K. J. D. MacKenzie, M. E. Smith and A. Wong, *J. Mater. Chem.*, 2007, **17**, 5090-5096.
52. K. Shimoda, Y. Tobu, K. Kanehashi, T. Nemoto and K. Saito, *Chem. Lett.*, 2005, **34**, 1588-1589.
53. K. Shimoda, Y. Tobu, K. Kanehashi, T. Nemoto and K. Saito, *Solid State Nucl. Magn. Reson.*, 2006, **30**, 198-202.
54. K. Shimoda, Y. Tobu, K. Kanehashi, T. Nemoto and K. Saito, *J. Non-Cryst. Solids*, 2008, **354**, 1036-1043.
55. K. Shimoda, Y. Tobu, Y. Shimoikeda, T. Nemoto and K. Saito, *J. Magn. Reson.*, 2007, **186**, 156-159.
56. F. Angeli, M. Gaillard, P. Jollivet and T. Charpentier, *Chem. Phys. Lett.*, 2007, **440**, 324-328.
57. K. Kanehashi, *Solid State Nucl. Magn. Reson.*, 2017.
58. I. L. Moudrakovski, R. Alizadeh and J. J. Beaudoin, *Phys. Chem. Chem. Phys.*, 2010, **12**, 6961-6969.
59. S. Chen, B. E. G. Lucier, M. Chen, V. V. Terskikh and Y. Huang, *Chem. Eur. J.*, 2018, **24**, 8732-8736.
60. D. Lee, C. Leroy, C. Crevant, L. Bonhomme-Coury, F. Babonneau, D. Laurencin, C. Bonhomme and G. De Paëpe, *Nat. Commun.*, 2017, **8**, 14104.
61. J. Xu, P. Zhu, Z. Gan, N. Sahar, M. Tecklenburg, M. D. Morris, D. H. Kohn and A. Ramamoorthy, *J. Am. Chem. Soc.*, 2010, **132**, 11504-11509.
62. H. Colas, L. Bonhomme-Coury, C. C. Diogo, F. Tielens, F. Babonneau, C. Gervais, D. Bazin, D. Laurencin, M. E. Smith, J. V. Hanna, M. Daudon and C. Bonhomme, *CrystEngComm*, 2013, **15**, 8840-8847.
63. D. Laurencin, C. Gervais, A. Wong, C. Coelho, F. Mauri, D. Massiot, M. E. Smith and C. Bonhomme, *J. Am. Chem. Soc.*, 2009, **131**, 13430-13440.
64. A. Wong, A. P. Howes, R. Dupree and M. E. Smith, *Chem. Phys. Lett.*, 2006, **427**, 201-205.
65. V. M. Sonje, L. Kumar, C. L. Meena, G. Kohli, V. Puri and R. Jain, *Atorvastatin calcium. Profiles of drug substances, excipients, and related methodology*, Elsevier In.2010.
66. E. S. Istvan and J. Deisenhofer, *Science*, 2001, **292**, 1160-1164.
67. H. G. Brittain and D. J. W. Grant, *Effect of polymorphism and solid-state solvation on solubility and dissolution rate*, Marcel Dekker, Inc, New York, 1999.
68. W. D. Wang, X. D. Gao, M. Strohmeier, W. Wang, S. Bai and C. Dybowski, *J. Phys. Chem. B*, 2012, **116**, 3641-3649.
69. M. Bak, J. T. Rasmussen and N. C. Nielsen, *J. Magn. Reson.*, 2000, **147**, 296-330.
70. E. A. Klop, A. Schouten, P. Vandersluis and A. L. Spek, *Acta Crystallogr. Sect. C-Cryst. Struct. Commun.*, 1984, **40**, 51-53.
71. U.S. Patent 5, 969, 156.
72. M. J. Frisch, G. W. Trucks, H. B. Schlegel, G. E. Scuseria, M. A. Robb, J. R. Cheeseman, G. Scalmani, V. Barone, B. Mennucci, G. A. Petersson, H. Nakatsuji, M. Caricato, X. Li, H. P. Hratchian, A. F. Izmaylov, J. Bloino, G. Zheng, J. L. Sonnenberg, M. Hada, M. Ehara, K. Toyota, R. Fukuda, J. Hasegawa, M. Ishida, T. Nakajima, Y. Honda, O. Kitao, H. Nakai, T. Vreven, J. A. Montgomery, J. E. Peralta, F. Ogliaro, M. Bearpark, J. J. Heyd, E. Brothers, K. N. Kudin, V. N. Staroverov, R. Kobayashi, J. Normand, K. Raghavachari, A. Rendell, J. C. Burant, S. S. Iyengar, J. Tomasi, M. Cossi, N. Rega, J. M. Millam, M. Klene, J. E. Knox, J. B. Cross, V. Bakken, C. Adamo, J. Jaramillo, R. Gomperts, R. E. Stratmann, O. Yazyev, A. J. Austin, R. Cammi, C. Pomelli, J. W. Ochterski, R. L. Martin, K. Morokuma, V. G. Zakrzewski, G. A. Voth, P. Salvador, J. J. Dannenberg, S. Dapprich, A. D. Daniels, Farkas, J. B. Foresman, J. V. Ortiz, J. Cioslowski and D. J. Fox, Wallingford CT2009.

73. T. H. Dunning, *J. Chem. Phys.*, 1989, **90**, 1007-1023.
74. J. P. Perdew, K. Burke and M. Ernzerhof, *Phys. Rev. Lett.*, 1996, **77**, 3865-3868.
75. R. Improta, V. Barone, G. Scalmani and M. J. Frisch, *J. Chem. Phys.*, 2006, **125**, 054103.
76. R. Improta, G. Scalmani, M. J. Frisch and V. Barone, *J. Chem. Phys.*, 2007, **127**, 074504.
77. A. V. Marenich, C. J. Cramer and D. G. Truhlar, *J. Phys. Chem. B*, 2009, **113**, 6378-6396.
78. S. Adiga, D. Aebi and D. L. Bryce, *Can. J. Chem.*, 2007, **85**, 496-505.

Table of Contents: Graph